Proceedings of CONF-MSS 2025 Symposium: Machine Vision System
DOI: 10.54254/2755-2721/2025.CH24657

Based on the Design Concept of a Bioinspired Continuum Robots with Programmable Stiffness Combined with a Nested Halbach Cylindrical Arrays in Exploration Activities

Yingpei Jiang

College of Engineering, Northeast Agricultural University, Harbin, China
j06y01p07@outlook.com

Abstract: As an important part of promoting social development, exploration activities are inevitably accompanied by certain risks in extreme environments or high-risk areas where exploration tasks are carried out. In order to reduce the threat to personnel safety in complex environments and improve the efficiency of exploration, the application of robotic technology can effectively enhance the robotic adaptability and flexibility in complex environments. In the Bioinspired Continuum robot with programmable stiffness designed for the trunk-like structure, the Intelligent Spring with Programmable Stiffness (ISPS), as a key element in the Cable-driven Continuum Robot (CCR), exhibits an excessively low bending speed during individual simulation tests. Therefore, this study proposes combining the nested Halbach cylindrical array structure with the CCR structure. Additionally, by installing small magnetic beads on the ISPS, it is proposed to enhance the bending efficiency of the ISPS through the action of magnetic force, thereby accelerating the bending efficiency of the robot to achieve higher usage efficiency in complex exploration environments. In this study, through the prediction of the data size of the equipment and the simulation calculations in the formulas, it is concluded that the device can generate a variable magnetic field and apply an additional magnetic force to a single ISPS. As a result, it is practically feasible to accelerate the bending efficiency of the ISPS. This innovation provides a practical improvement scheme for similar bionic robots in terms of increasing the bending speed and thus enhancing the exploration efficiency.

Keywords: Exploration, Elephant Trunk-like Robot, Variable Magnetic Field, Low-Melting-Point Alloy, Structural Design

1. Introduction

In today's rapidly developing world, various types of explorations are taking place continuously, such as topographic exploration, rescue exploration, mineral exploration, and so on. The use of various robots enables adaptation to complex and dangerous exploration environments, thereby reducing the risk of injury associated with these conditions. Nowadays, a variety of special upgrading and transforming robots have been developed, enabling them to specially adapt to specific environments. For example, underwater robots that play an important role in marine resource exploration, environmental monitoring and protection, and auxiliary construction [1], programmable shaped

© 2025 The Authors. This is an open access article distributed under the terms of the Creative Commons Attribution License 4.0 (https://creativecommons.org/licenses/by/4.0/).

DOI: 10.54254/2755-2721/2025.CH24657

hydrogel fibers that can cope with solvents and ambient humidity [2], and fuzzy control algorithms designed in balanced robots for improved responsiveness, robustness and stability [3].

One of them is the Intelligent Spring with Programmable Stiffness (ISPS), which is composed of low-melting-point alloy (LMPA) as the key material, and it has become a crucial structure of the Bioinspired Continuum robot. Nowadays, the applications of low-melting-point alloys have been extremely extensive. For example, in the process of forming the tooling for shaped composite parts, the use of low-melting-point alloys can improve the dimensional and surface accuracy of the parts [4]. By utilizing the penetration mechanism of low-melting-point alloy in wood, metalized poplar wood is prepared, which enhances its compressive strength along the grain and shows good application prospects in the field of geothermal floor heating [5]. And in order to solve the heat dissipation problem of electronic devices when they operate with short-term dynamic high power in an environment without wind and liquid, a low-melting-point alloy phase change heat sink with a heat conducting fin structure was proposed [6]. The low-melting-point alloy used in this paper is Cerrolow 147, which belongs to the bismuth-tin alloy. Its melting point is 47°C, and its physical properties are stable in the molten state, with excellent cooling characteristics [7]. When heated, the low-melting-point alloy changes from a solid state to a liquid state, causing the ISPS to soften. When cooled, the alloy solidifies, and the ISPS regains its rigidity. This endows the robot with the characteristic of programmable stiffness, which is of great significance in the design and performance realization of continuum robots. The bionic Continuum robot makes use of the characteristics of low-melting-point alloys and the key structure of the elephant trunk, enabling it to handle scenes with different curvatures. It overcomes the limitations of existing continuum robots by programming the structural stiffness [8]. During the exploration process, the reaction rate is of vital importance and is one of the key factors affecting efficiency [9]. However, in the heating and softening experiment of the ISPS part of the bionic Continuum robot, under the single cantilever beam configuration, when it bears a weight of 50 g, the slight displacement at the tip is 0.53 ± 0.12 mm. When heated by Joule heating (T > Tm of 47 °C), the LMPA will undergo a phase transition from solid to liquid, softening the ISPS, which in turn leads to a large bending deformation at an angle of 90.17° ± 5.32° under the same weight. It takes about 8 minutes for the ISPS to complete the large bending deformation from the start of heating when it bears a weight of 50 g. While after removing the 50 g load, it takes about 10 minutes from the start of heating to approach the restoration of the initial position [8]. Obviously, the speed of the bending change is too slow and the efficiency is too low, which may not be able to meet the purpose of making quick turns during the exploration process, thus affecting the reaction speed of the final overall machinery.

Therefore, the aim of this article is to propose a concept of a design similar to that of the Variable single-axis magnetic-field generator, which is nested on the basis of the ISPS in Continuum robots [10]. Through the prediction of the data size of the equipment and the simulation calculations in the formulas, it is concluded that this device can generate a variable magnetic field and apply an additional magnetic force to a single ISPS. This can increase the bending speed of the ISPS structure when it is heated, softened and subjected to force, thereby enhancing the overall adaptability and usage efficiency of this mechanism in complex exploration environments, and providing a practical vision for the development of future bionic robots [11].

2. Literature review

2.1. Principles and defects of programmable stiffness bioinspired continuum robot

Based on the structural characteristics of the elephant trunk, Zhang designed the Cable-driven Continuum Robot(CCR), which is applied as a key structure in a bioinspired continuum robot with programmable stiffness. The CCR is composed of 12 modular tensegrity structures and is divided

DOI: 10.54254/2755-2721/2025.CH24657

into three independently controllable segments [8]. The power source selectively supplies current to each segment. Through the current, the structural stiffness of each segment can be actively adjusted, enabling the CCR to exhibit eight stiffness sequences. Then, each segment is actuated by heating or cooling the Intelligent Spring with Programmable Stiffness(ISPS), allowing the CCR to still show different profiles after deformation. As a result, it can be applied to various deformation scenarios [8]. Among them, the ISPS is composed of low melting point alloy (LMPA) as the key material, copper wires as the conductors, and silicone rubber tubes(Figure 1). When the wire is energized and heats up to reach the liquefaction temperature of the LMPA, the ISPS undergoes deformation under the action of the pulling force. As a result, after the segmented regulation, the CCR can exhibit different morphologies.

In the experiment to separately test the performance of the ISPS, the horizontally fixed ISPS structure, under the combined action of the vertical pulling of a 50g weight and heating softening, took about 8 minutes to bend from zero to 90°. Moreover, the natural recovery process took as long as about 10 minutes [8]. However, during the actual survey process, the robotic arm often encounters places where large and rapid turns are required. The original ISPS device has too low efficiency, which is likely to lead to the failure of some urgent survey tasks. Therefore, improving the bending efficiency of the ISPS is the central focus of this design.

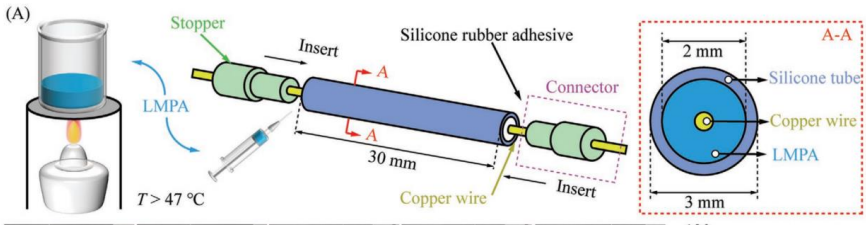

Figure 1: A Diagram of the structural composition of ISPS

2.2. The principle of nested Halbach cylindrical arrays adopted for deficiencies

To improve the bending efficiency of the ISPS, this paper adopt nested Halbach cylindrical arrays composed of Halbach arrays, shown in Figure 2. Magnets with different orientations are arranged according to a certain pattern, causing the magnetic field lines on one side to converge and those on the other side weaken, thereby obtaining a relatively ideal unilateral magnetic field [12].

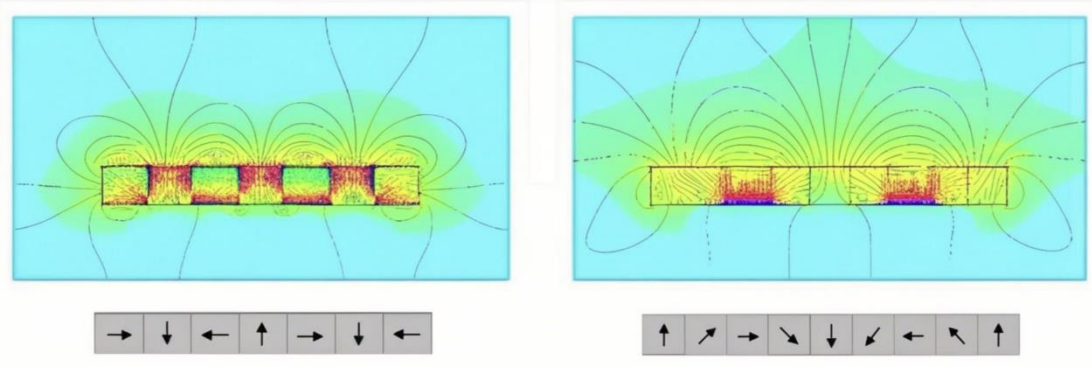

Figure 2: The Halbach array and schematic diagram

The circular Halbach array can be regarded as a circular ring shape formed by connecting the head and the tail of the linear Halbach array [10]. As shown in Figure 3, the annular Halbach arrays that are arranged in different rule can provide different forms of magnetic field directions. This

DOI: 10.54254/2755-2721/2025.CH24657

characteristic of the unilateral magnetic field enables the circular Halbach array to generate a magnetic field inside while not generating a magnetic field outside. Therefore, it has no impact on the external mechanical structure, and the internal magnetic field can serve as the magnetic field for the CCR component of the bionic elephant trunk mechanism.

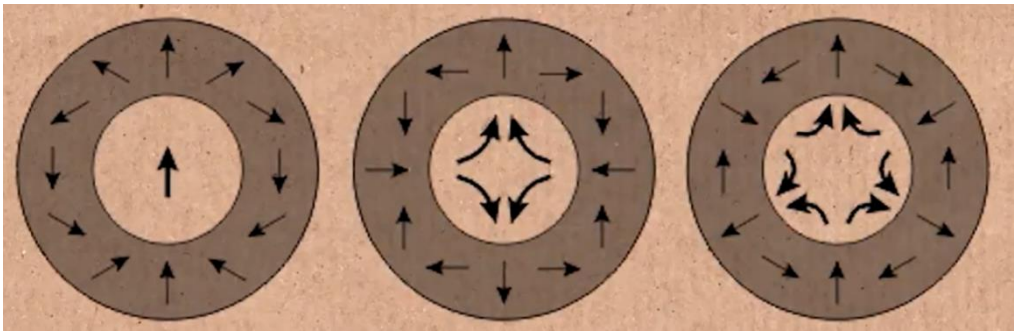

Figure 3: schematic diagram of the annular Halbach array

The principle of this Variable single-axis magnetic-field generator is that, based on the superimposed application of the Halbach array, the magnetic field can be regulated by rotating the inner and outer Halbach arrays to the corresponding relative positions [10]. As shown in Figure 4, in the left diagram, the directions of the outer ring and the inner ring are the same, and the overlapping magnetic fields show an enhancement, achieving the effect of enhancing the internal magnetic field. In the right figure, the directions of the outer ring and the inner ring are opposite, causing the overlapping magnetic fields to cancel each other out, achieving the effect of weakening the internal magnetic field. This device can provide a stronger magnetic field when the magnetic field is required. When the magnetic field is not needed, it can offset the magnetic field to achieve the effect that the internal magnetic field is zero. In this way, when the magnetic field is not required, it can prevent the magnetic field from affecting the operation of the machinery. The device as a whole achieves a unilateral magnetic field, so it can avoid the influence of the external magnetic field of the device on external machinery during its operation.

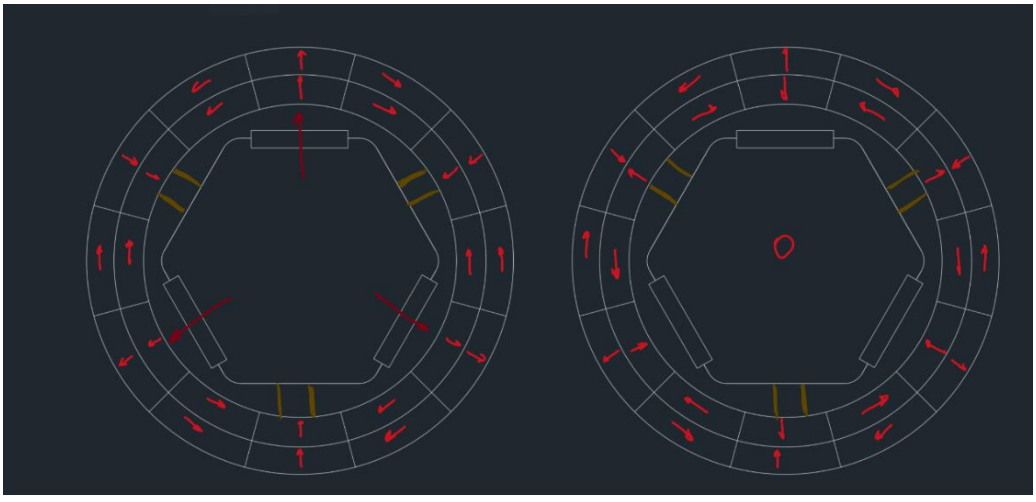

Figure 4: The magnetic field arrangement when the nested Halbach cylindrical arrays is applied to the CCR; Left. Schematic diagram when the magnetic field directions of the outer ring and the inner ring are the same; Right. Schematic diagram when the magnetic field directions of the outer ring and the inner ring are opposite

DOI: 10.54254/2755-2721/2025.CH24657

3. Methodology

3.1. The magnetic force increases the bending speed of the ISPS under force

For an ideal cylindrical Halbach dipole, considering it as an infinitely long tube, the calculation formula for the magnetic field strength it generates in the cross-sectional plane is as follows:

$$B_{outer} = B_{rem} * \ln\left(\frac{r_1}{r_2}\right) \tag{1}$$

Among them, $B_{rem}$is the remanence of the permanent magnetic material, and its magnitude is $B_{rem} \approx 14kg$. r_1 and r_2 are the outer radius and the inner radius of the tube, respectively. In the case of a nested Halbach dipole, the magnetic field strength generated by the inner dipole is:

$$B_{inner} = B_{rem} * \ln\left(\frac{r_3}{r_4}\right) \tag{2}$$

When $r_3 = r_2$ and $r_4 = \frac{{r_2}^2}{r_1}$ are satisfied, $|B_{outer}| = |B_{inner}|$, and the central synthesized magnetic field is [10]:

$$B_{tot} = B_{outer} + B_{inner} \tag{3}$$

In this way, the magnitude and variation range of the magnetic field generated by the nested Halbach dipole pairs can be theoretically analyzed. According to the dimensions in Figure 4, a single hexagonal ring-shaped layer is alternately connected by three rigid crossbars (with a length of $Lt = 30mm$) and three ISPSs (with a length of $Ls = 30mm$). In this design, $r_4 = 35mm$ and $r_3 = 45mm$. According to the formula above, $r_2 = 45mm$ and $r_1 = 57.85mm$. At these dimension, it can meet the requirement that when the magnetic field arrangement sequences of the inner ring and the outer ring are opposite, the central magnetic fields cancel each other out, achieving the effect that the intensity of the central magnetic field is 0. However, under these designed dimension, the calculated results show that $B_{outer} = 3.52kg$ and $B_{inner} = 3.52kg$. According to the formula $B_{tot} = B_{outer} + B_{inner}$, the magnitude of the central synthesized magnetic field is equal to 7.04 kg, which is equivalent to 0.704T.

In addition, according to the definition of the magnetization intensity M,

$$M = Vm \tag{4}$$

Among them, m is the magnetic moment and V is the volume.

For a spherical sample, r represents the radius of the small magnetic bead, and $V = 4/3\,\pi r^3$。Since the relationship between the magnetization intensity M and the magnetic field intensity $H = \mu_0 B, \mu_0 = 4\pi \times 10^{-7} T\,m/A$ is given by:

$$M = \chi H \tag{5}$$

Where χ represents the magnetic susceptibility.

Since $V = 4/3\,\pi r^3$, and $M = \chi H$, it can be obtained that: $\chi H = {}^{m}/_{4/3\,\pi r^3}$, and, $m = 4/3\,\pi r^3 \chi H$. Therefore, for a uniformly magnetized small magnetic bead, the magnetic moment is calculated according to the formula $m = 4/3\,\pi r^3 \chi H$. It is assumed that the radius of the small magnetic bead $r = 1 \times 10^{-3} m$, and when the small magnetic bead is made of soft magnetic material, the magnetic susceptibility $\chi = 0.1$ [13].

DOI: 10.54254/2755-2721/2025.CH24657

According to the relationship between the magnetic induction intensity B and the magnetic field intensity H in a vacuum,

$$B = \mu_0 H \tag{6}$$

Where B is the magnetic induction intensity, with the unit of Tesla (T). μ_0 is the magnetic permeability of vacuum, and $\mu_0 = 4\pi \times 10^{-7} T \cdot m/A$. H is the magnetic field strength, with the unit of A/m. By transformation, we can obtain:

$$H = \frac{B}{\mu_0} \tag{7}$$

Substitute the magnitude of the centrally synthesized magnetic field, then:

$$H = 0.704T/4\pi \times 10^{-7} T \cdot m/A \approx 5.6 \times 10^5 \, A/m \tag{8}$$

$$m = 4/3\pi \times \left(1 \times 10^{-3} m\right)^3 \times 0.1 \times 5.6 \times 10^5 \, A/m \approx 2.35 \times 10^{-6} A \cdot m^2 \tag{9}$$

Calculate the magnetic force by combining with the magnetic field gradient. If the magnetic field gradient $dB/dz = 1T/m$, the magnetic force received is

$$F = mdB/dz \cos\theta \tag{10}$$

Where θ is the angle between the magnetic moment m and the direction of the magnetic field gradient (here it is the z-direction).

Under the assumption that the direction of the magnetic moment m is parallel to the direction of the magnetic field gradient, that is, $\theta = 0^\circ$ and $\cos\theta = 1$, then [14]:

$$F = 2.35 \times 10^{-6} A \cdot m^2 \times 1 \, T/m = 2.35 \times 10^{-6} N \tag{11}$$

Therefore, a single small magnetic bead can provide a magnetic force of $2.35 \times 10^{-6} N$ in this magnetic field. According to Figure 5 and Figure 6, six small magnetic beads with a radius of $r = 1 \times 10^{-3} m$ can just be arranged in a circle around the outside of an ISPS with the same radius. They are designed to be arranged around the middle position of the ISPS, that is, a total of 24 small magnetic beads are arranged. Therefore, a magnetic force of $5.64 \times 10^{-5} N$ can be generated and act on the ISPS to accelerate the bending speed of the ISPS.

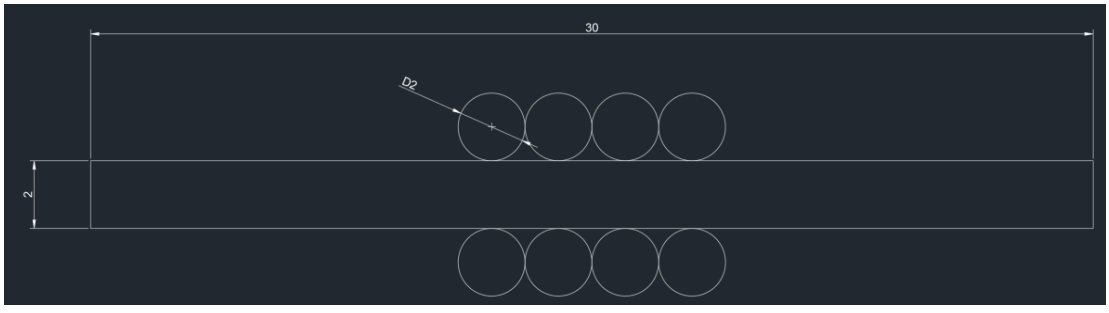

Figure 5: Simulation diagram of installing small magnetic beads at the middle position of a single ISPS

DOI: 10.54254/2755-2721/2025.CH24657

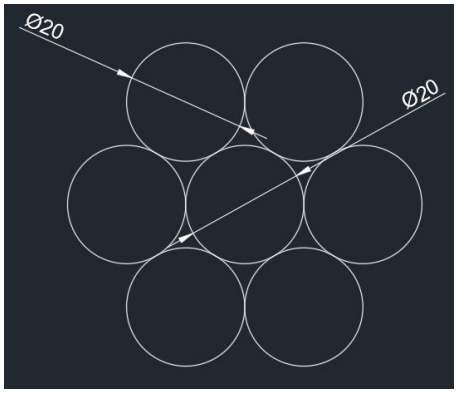

Figure 6: Sectional view of a single hexagonal ring layer on the ISPS after installing small magnetic beads

3.2. The nested Halbach cylindrical arrays can provide a variable magnetic field for the ISPS of the small magnetic beads nested in the middle.

The nested Halbach cylindrical array is connected to the CCR in the manner shown in Figure 4. Figure 6 illustrates the sectional view of a single hexagonal ring-shaped layer on the CCR. Through the dimensional design of the double-layer ring, the magnitudes of the magnetic fields generated by the inner and outer rings are made to be the same, that is, $\left|B_{outer}\right| = \left|B_{inner}\right|$, and $B_{outer} = B_{inner} = 3.52kg$ [14]. In the case of the left diagram in Figure 4, the magnetic field arrangement sequences of the outer ring and the inner ring are the same. According to the characteristics of the Halbach array, the magnetic fields on the inner side are combined and enhanced, so that $B_{tot} = B_{outer} + B_{inner}$ reaches the maximum. The magnitude of the synthesized magnetic field at the center is equal to $7.04kg$. Moreover, according to the special arrangement sequence, the enhancement points of the three magnetic fields can exactly pass through the three ISPS structures, amplifying the magnetic force effect. In the case of the right diagram in Figure 4, the magnetic field arrangements of the outer ring and the inner ring are opposite. According to the characteristics of the Halbach array, the magnetic fields on the inner side are combined and cancelled out, so that the magnitude of the minimum central resultant magnetic field obtained from the equation $B_{tot} = B_{outer} + B_{inner}$ is exactly 0 [14]. Additionally, the characteristics of the Halbach array make it such that when the magnetic field directions of the inner and outer rings are opposite (Figure 4, Right), there is no magnetic field on both the inner and outer sides of the double-ring.

Upon observation, when the magnetic field directions of the inner and outer rings are opposite (Figure 4, Right), it is precisely obtained by rotating the state when the magnetic field directions of the inner and outer rings are the same (Figure 4, Left) 60° to the right. Therefore, the inner and outer rings can be positioned at different locations by controlling the angle of rotation. When the angle varies between 0° and 60°, a gradually decreasing magnetic field can be generated, thereby providing the nested Halbach cylindrical array provides a variable magnetic field for the ISPS of the small nested magnetic bead in the middle. Finally, this variable magnetic field is utilized. It can achieve the following function: when the magnetic force is required to accelerate the bending of the ISPS, the magnetic field can be provided. When the magnetic force is not needed, the magnetic field can be turned off. In this way, the generation of an excessive magnetic field that might affect other components can be prevented.

DOI: 10.54254/2755-2721/2025.CH24657

4. Discussion

In this paper, a nested Halbach cylindrical array is combined with the CCR part of the bionic elephant trunk. Small magnetic beads are added to the ISPS within the CCR. In this way, magnetic force can be generated under the action of a magnetic field and act on the ISPS. By accelerating the bending deformation of the ISPS, the deformation efficiency of the entire CCR is increased, thereby accelerating the overall work efficiency of exploration. In the research on the methods of providing force, shape memory alloys can also be employed. By reaching their phase transition temperature, the shape memory alloys will recover their original shapes, thereby providing a pulling force to the ISPS, which is a way to accelerate the bending efficiency of the ISPS. However, the phase transition temperature of shape memory alloys is related to their specific types, compositions, processing techniques, and usage requirements. The control over the applied force is relatively weak, and this material cannot be used to conduct relevant result tests through simulation. In addition, a temperature-related low melting point alloy (LMPA) was also involved in the fabrication of the ISPS. However, the situation of using LMPA in combination with shape memory alloys imposes relatively high requirements on the experimental conditions, which cannot be met currently. Therefore, in this design, priority is given to completing the relevant design based on the provision of force by means of magnetic force and a variable magnetic field. Since the electromagnet controls the magnitude of the magnetic force through electricity, taking into account the large variety of electrical components available for selection, the requirements for the arrangement and use of wires, practicality, the difficulty of controlling the generation of a magnetic field in a single direction, the need for equipment simplification, and the impact of the excess magnetic field on other equipment, etc., this paper designs a Halbach array as the component for providing the magnetic field effect, which stabilizes the supply of the magnetic force and ensures the correct operation of the equipment. The application of the Halbach array is quite common in daily life. For instance, the single-sided magnetic attraction of refrigerator magnets. Therefore, the manufacturing cost of this nested Halbach cylindrical array is not high, and its size is relatively small. It can be well integrated with the CCR without appearing cumbersome. Therefore, in this study, the nested Halbach cylindrical arrays are utilized to provide the magnetic field effect. This approach can achieve the effect of providing a variable magnetic field without generating any excessive magnetic field to the outside environment, which is highly suitable for the bionic elephant trunk manipulator, the main subject of this study, and its working environment.

5. Conclusion

In the exploration environment, in order to enhance the working ability of the Bioinspired Continuum robot with programmable stiffness of the biomimetic elephant trunk and improve the work efficiency, this article combines the nested Halbach cylindrical arrays and utilizes the characteristics of the Halbach array to act on the CCR part of the target elephant trunk robot. In this way, a magnetic force is provided for the ISPS (which is installed with small magnetic beads), thereby accelerating the bending efficiency of the ISPS, and finally achieving an improvement in the efficiency of the exploration work. However, this concept still has its drawbacks. Firstly, the magnetic field provided by this method is still relatively weak, resulting in a small generated force. It is necessary to discuss how to provide a stronger magnetic field to further enhance the bending effect of the ISPS. In the second aspect, since the CCR is composed of multiple single hexagonal ring-shaped layers, and in order to achieve bending, it is inevitable that there will be gaps between the adjacent two layers of hexagonal ring-shaped layers for the nested Halbach cylindrical arrays. However, the generation of these gaps may lead to the leakage of the internal magnetic field to the outside of the machinery, which may affect the operation of other unrelated machinery. In the future, the development of robots in the exploration field will still be popular, and the significance of robot development in the

DOI: 10.54254/2755-2721/2025.CH24657

exploration field will remain extremely substantial. There is still a vast development space for this trunk-like robot, and there are still numerous ways to enhance the working efficiency of robots. In terms of improving the bending efficiency of the ISPS, in the future, it is possible to attempt to use shape memory alloys and replace the low-melting-point alloy of the central material, so as to improve the overall bending efficiency of the ISPS. There is also room for improvement in the way the magnetic field is provided and in the form and material of the small magnetic beads, so that they can work together to achieve a greater magnetic force effect.

References

[1] *Tang Z.S.H.(2024). Innovation and Practice of Underwater Robot Technology in Marine Engineering[J]. Pearl River Water Transport. (6): 108-110. DOI:10.14125/j.cnki.zjsy.2024.06.005.*

[2] *Zhai, Y.D., Gong, C., Chen, J.H. & Chang,C.Y. (2023). Magnetic-field induced asymmetric hydrogel fibers for tough actuators with programmable deformation, Chemical Engineering Journal. Vol. 477, 147088., DOI:10.1016/j.cej.2023.147088.*

[3] *Liu H., Li Z., Yang M.H., Deng X.G. & Cao Y.P. (2023). Design of a Full-Displacement Balanced Robot Based on Fuzzy Control[J]. Measurement & Control Technology. 42(7): 102-109.DOI:10.19708/j.ckjs.2022.08.298.*

[4] *Cao C., Hong X.M. & Dang X.L. (2025). Application of Low-Melting-Point Alloys in the Forming Tooling of Special-Shaped Composite Parts [J]. Die & Mould Manufacture. 25(01): 25-26 + 29. DOI:10.13596/j.cnki.44-1542/th.2025.01.008.*

[5] *Sun Y.P., Yu X.D., Chai X.J., Xu, K.M. & Xie L.K. (2024). Study on the Properties and Mechanism of Poplar Wood Impregnated by Low-Melting-Point Alloy under High and Low Temperature Cycling [J]. China Forest Products Industry. 61(04): 1-6. DOI:10.19531/j.issn1001-5299.202404001.*

[6] *Chen X.C., Huang G.C. & Gu Z.C. (2024). Research on the Design and Heat Dissipation Performance of a Low-Melting-Point Alloy Phase Change Heat Sink [J]. Electro-Mechanical Engineering. 40(04): 22-27. DOI:10.19659/j.issn.1008-5300.2024.04.006.*

[7] *Dušek, K., Bušek, D., Veselý, P., Pražanová, A., Plaček, M. & Re, J.D. (2022). Understanding the Effect of Reflow Profile on the Metallurgical Properties of Tin–Bismuth Solders. Metals. 12, 121. DOI:10.3390/met12010121.*

[8] *Zhang, J., Wang, B., Chen, H., Bai, J., Wu, Z., Liu, J., Peng, H. & Wu, J. (2023). Bioinspired Continuum Robots with Programmable Stiffness by Harnessing Phase Change Materials. Adv. Mater. Technol. 8, 2201616. DOI:10.1002/admt.202201616.*

[9] *Mu X.H. & Ding Y. (2024). Exploration on the Application of Comprehensive Geological Exploration Methods [J]. Inner Mongolia Coal Economy. (22): 181-183. DOI: 10.13487/j.cnki.imce.026051.*

[10] *Tretiak, O., Blümler P. & Bougas, L. (November, 2019). Variable single-axis magnetic-field generator using permanent magnets. AIP Advances. 9(11): 115312. DOI:10.1063/1.5130896.*

[11] *Zhang X.F., Wu Z.Y., Xu X.R., Zhang, E., Wei, S.B. & Xie, F. (2024). Research on a Quadruped Bionic Robot for Intelligent Exploration and Rescue in Air and on Land in Complex Terrains [J]. Automation Application. 65(15): 31-34+37. DOI: 10.19769/j.zdhy.2024.15.009.*

[12] *Li C., Hong Q., Yang X.B., Chen, R., Sun, Y.D. & Liang, L.L. (2021). Numerical Simulation Based on C++ of the Magnetic Field Distribution and Magnetic Induction Lines of a Circular Current [J]. Physical Experiment of College. 34(03): 28-30. DOI: 10.14139/j.cnki.cn22-1228.2021.03.008.*

[13] *Zhan Y.Z., Pan Y.F., Huang J.F., Liang J. & Wang X.Z. (2015). Research Progress in the Application of Soft Magnetic Materials[J]. Guangxi Sciences. 22(5): 467-472. DOI:10.13656/j.cnki.gxkx.20151027.017.*

[14] *Qin W.N., Wei L.X. & Jia X.L. (2024). Preparation of Fe3N Magnetic Nanoparticles and Research Progress of Their Applications [J]. Chemical Engineer. 38(01): 61-65+74. DOI: 10.16247/j.cnki.23-1171/tq.20240161.*